

Synthesis of Encapsulated Titanium Oxide Sodium 2-Acrylamido-2-methylpropan Sulfonate Nanocomposite for Preventing the Corrosion of steel

G. A. El-Mahdy^{1,2,*}, A. M. Atta^{1,3}, H. A. Al-Lohedan¹, A. M. Tawfeek⁴, Ahmed A. Abdel-Khalek⁵

¹Surfactants research chair, Department of Chemistry, College of Science, King Saud University, P.O.Box 2455, Riyadh 11451, Saudi Arabia

²Chemistry department, Faculty of Science, Helwan University, Helwan 11795, Egypt

³Petroleum application department, Egyptian petroleum research institute, Nasr city 11727, Cairo, Egypt.

⁴College of Science, King Saud University, Riyadh, Saudi Arabia.

⁵Chemistry department, Faculty of Science, Beni Suf University, Beni Suf, Egypt.

*E-mail: gamalmah2000@yahoo.com

Received: 11 February 2015 / Accepted: 27 April 2015 / Published: 27 May 2015

Poly(Sodium-2-Acrylamido-2-methylpropane) Sulfonate, PNa-AMPS nanocomposite consisting of a nanocrystalline titania matrix was prepared by suspension of the titania particles followed by crosslinking radical polymerization of Na-AMPS monomer. The chemical structure of the prepared nanogel was evaluated by FTIR. The crystallinity, morphology and particle size distribution were characterized by XRD patterns, TEM and DLS analyses. The high corrosion inhibition effectiveness of TiO₂ nanoparticles in chloride containing environment is reported using electrochemical techniques. All measurements showed that TiO₂ nanoparticles had excellent corrosion protection for the corrosion of steel in acidic chloride solution and the protection efficiency is strongly dependent upon inhibitor concentration. Polarization data reveal that TiO₂ nanoparticles act as a mixed-type inhibitor.

Keywords: Corrosion EIS Polarization, inhibition

1. INTRODUCTION

Nano-structured TiO₂ (titania) thin film acts as important nanomaterial from the technological point of view due to its outstanding properties as good chemical stability, unique photoelectrochemical properties, biocompatibility and high corrosion resistance. Titania is antimicrobial material acts as photo catalytic materials to degrade several hazardous materials. TiO₂ has several industrial

applications as coating composites for self-cleaning windows, dye-sensitized solar cells, water electrolysis for solar energy conversion and as anti-corrosion materials [1–7]. In addition, TiO₂ coating had been employed as a cathodic protection of substrate under UV illumination [8]. The main disadvantage of nano-structured TiO₂ is referred to dispersion in the solutions and organic coatings that can be enhanced using surfactants or conversion to amphiphilic nanogel materials [5-7].

Many researchers have been developed a novel strategy for the corrosion prevention of the metals by covering the substrates with TiO₂ films [9-11]. The photocathodic protection achieved by TiO₂ or TiO₂-based composite films on various substrates has been widely employed in industrial applications [12–19]. A rapid fabrication of TiO₂ nanotubes by electrochemical reaction anodization has been extensively studied under breakdown conditions [20–22]. TiO₂ nanotubes have been previously employed as potential candidates for protection of underlying substrate [23–25]. It has been reported previously that TiO₂ can successfully offered photocathodic protection and corrosion inhibition to weathering steel [26], carbon steel [27-29] and stainless steel [30-32]. The agglomeration of TiO₂ affects the electrochemical reactions that needs to disperse TiO₂ in the solutions or coatings. In this respect, the aim of this work is to synthesis amphiphilic crosslinked nano-polymer composite in the presence of TiO₂ nanoparticles (NPs) to increase their surface activity in organic and aqueous solutions. The dispersed TiO₂ nanogel composite is used for preventing the corrosion of steel in acidic chloride environment using different electrochemical techniques.

2. EXPERIMENTAL

2.1 Materials

Titanium oxide nano-powder was produced from Sigma-Aldrich Co. with average particle size 21 nm. Na AMPS is used as anionic monomer to coat TiO₂ nanoparticles. PVP is used as dispersing agent to complete dispersion crosslinking polymerization. MBA is used as crosslinker for Na AMPS monomer. Ammonium persulfate (APS) used in conjugation with TEMED as initiator and activator, respectively for crosslinking radical polymerization at low temperature. All chemical were purchased from Sigma Chemicals. The chemical composition, the method of preparation of the working electrode, the reference and the counter electrode are the same as used previously in our studies [33-34]

2.2. Method of preparation

Free radical copolymerization technique used to produce the nanogel latex based Na-AMPS monomer and MBA crosslinker. The preparation technique is based on the following procedure: 50 mL of ethanol water mixture (EtOH/H₂O; 2/1 volume ratio) used to disperse 0.125 g of TiO₂ nano-powder in the presence of 0.5 g PVP. The mixture was mixed for 2 h. The monomer mixtures Na-AMPS (1.2 g) and MBA (28.3 μ l) were added dropwise to dispersed solution of titania under nitrogen

atmosphere. 0.0125 g KPS initiator and 20 μ l TEMED were introduced to the reaction mixture under at 10 °C during the last stage of reaction. The crosslinking polymerization was allowed to continue at 25 °C for 24 h. The TiO₂ nanogel solution is centrifuged to produce PNa-AMPS / TiO₂ nanogel composite.

2.3. Characterization of PNa-AMPS / TiO₂ nanogel

The chemical structure and interactions between TiO₂ and PNa-AMPS is performed using Fourier Transform infrared (FTIR).

The morphology of PNa-AMPS / TiO₂ nanogel is determine using HR-TEM; JEM-2100 F.

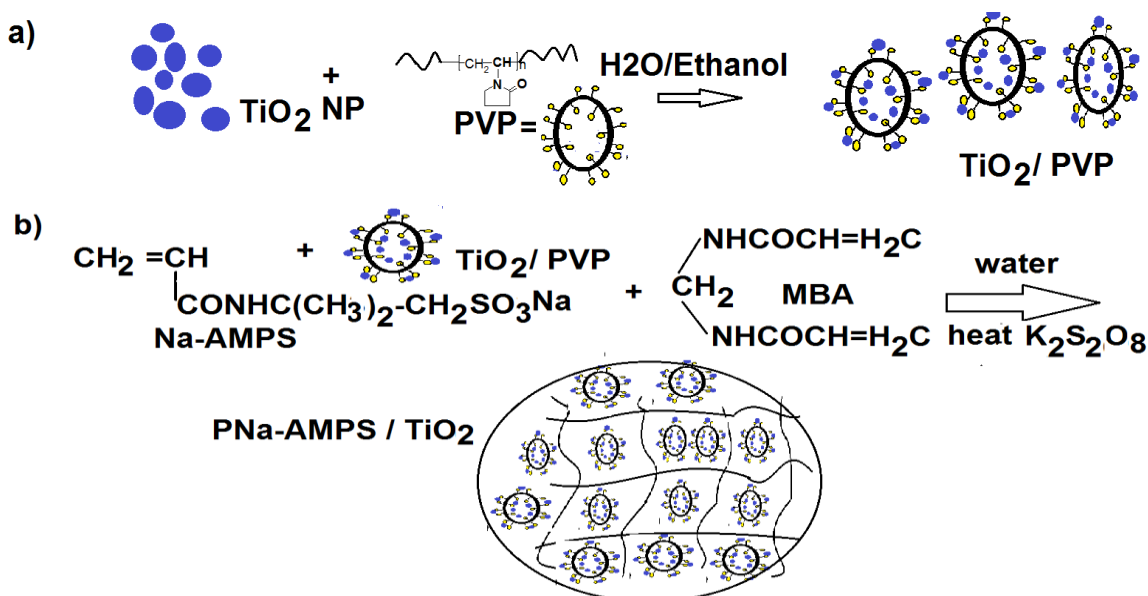
The crystal structure of PNa-AMPS / TiO₂ nanogel is confirmed by X-ray powder diffraction (XRD; X'Pert, Philips, Netherlands).

2.4. Electrochemical Measurements

Electrochemical experiments were performed using a potentiostat/galvanostat Solartron 1470E system. Polarization curves were conducted using a scan rate of 1mV/s after 1 h immersion in 1M HCl (uninhibited solution) and inhibited solutions. EIS data were conducted over a frequency range from 10KHz to 10 mHz. All electrochemical data were collected and analyzed using software package developed by Scribner Associates, Inc (UK)

3. RESULTS AND DISCUSSION

The present work objective directed to synthesise core/shell titania encapsulated into nanogel to increase their dispersability as nanomaterial to form thin film layer on steel to apply as corrosion inhibitor in aqueous acid solutions. Venkatachari et al. [35] reported that the ability of ions corroded the steel surface were inhibited in the presence of nanocomposite materials. Moreover, the presence of TiO₂ nanoparticle (NP) in organic coatings increases the charge resistance of the coatings [35]. In the present study, the dispersion polymerization technique used to encapsulate TiO₂ into nanogel composite based on PNa-AMPS in the presence of PVP as stabilizer as illustrated in the experimental section. Excellent of core shell TiO₂/PNa-AMPS colloidal stability was occurred using PVP as stabilizer. Excess PVP stabilizer content during polymerization of AMPS may cause nucleation to precipitate TiO₂/PNa-AMPS nanocomposite. Moreover, Too low concentration of PVP stabilizer could be insufficient to stabilize nanogel and causes coalescence and precipitation of TiO₂/PNa-AMPS nanocomposite. The composition of the materials was 3 wt% of TiO₂ with respect to the PNa-AMPS. The steps of the synthesis of PNa-AMPS/ TiO₂ nanogel were represented in the **Scheme 1**.



Scheme 1. Preparation of PNa-AMPS/ TiO_2 nanogel.

Scheme 1 indicates that more TiO_2 NPs can be encapsulated in the core of the crosslinked PNa-AMPS synthesized in the presence of PVP as stabilizer. As shown in scheme 1 a, in the presence of PVP, the amide groups of PVP are adsorbed onto TiO_2 NPs. Moreover, SO_3 groups of PNa-AMPS assist to encapsulate of TiO_2 NPs as core in the crosslinked networks as shell. FTIR, XRD and TEM analyses were employed to confirm the above reactions.

3.1. Chemical Structure of PNa-AMPS/clay nanogel

The chemical structures of TiO_2 nano-powder, PNa-AMPS/ TiO_2 nanogel were identified using FTIR absorption spectra as illustrated in Figure 1. The spectrum of the blank titania nano-powder, Figure 1a, shows two different stretching vibrations, one at 3740 cm^{-1} , that attributed to the OH groups, and one at 3680 cm^{-1} , referred to more acid OH groups. The band at 3740 cm^{-1} is assigned to the anatase phase [36]. These bands were disappeared after crosslinking polymerization of PNa-AMPS with titania nano-powder (Figure 1 b), a clear. It is obvious from the spectrum of PNa-AMPS/ TiO_2 nanogel that PNa-AMPS nanogels are attached to the acidic OH group located on the surface of titanium oxide as the band at 3680 cm^{-1} almost disappeared. Moreover, the other bands present at 1580 cm^{-1} , is assigned to TiO_2 -PVP. The FTIR spectrum of PNa-AMPS/ TiO_2 nanogel, represented in Figure 1b, showed bands in the range of $3400\text{--}3700 \text{ cm}^{-1}$ which are referred to the vibrational stretching of $-\text{OH}$ of clay and NH vibrational stretching of MBA and Na-AMPS. The bands at 1090 cm^{-1} and 1643 cm^{-1} referred to SO and CONH stretching of Na-AMPS, indicated the formation of PNa-AMPS gels. The disappearance of the $-\text{OH}$ stretching of various titania in the range of $3400\text{--}3700 \text{ cm}^{-1}$ indicated the encapsulation of titania into the PNa-AMPS polymeric networks [37].

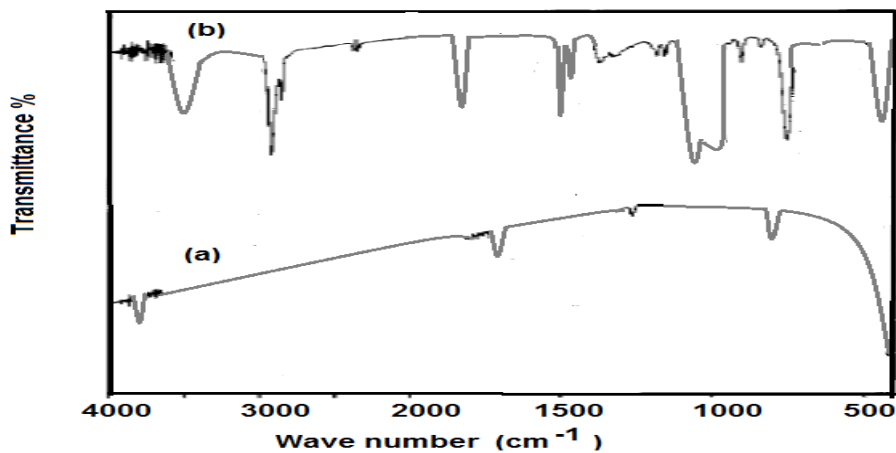


Figure 1. FTIR spectra of a) TiO₂ NPs b) PNa-AMPS/TiO₂ nanogel.

3.2. XRD analysis of PNa-AMPS/clay nanogel

The via X-Ray powder diffraction (XRD) can be used to study the phases and purity of the prepared PNa-AMPS /TiO₂ nanogels.

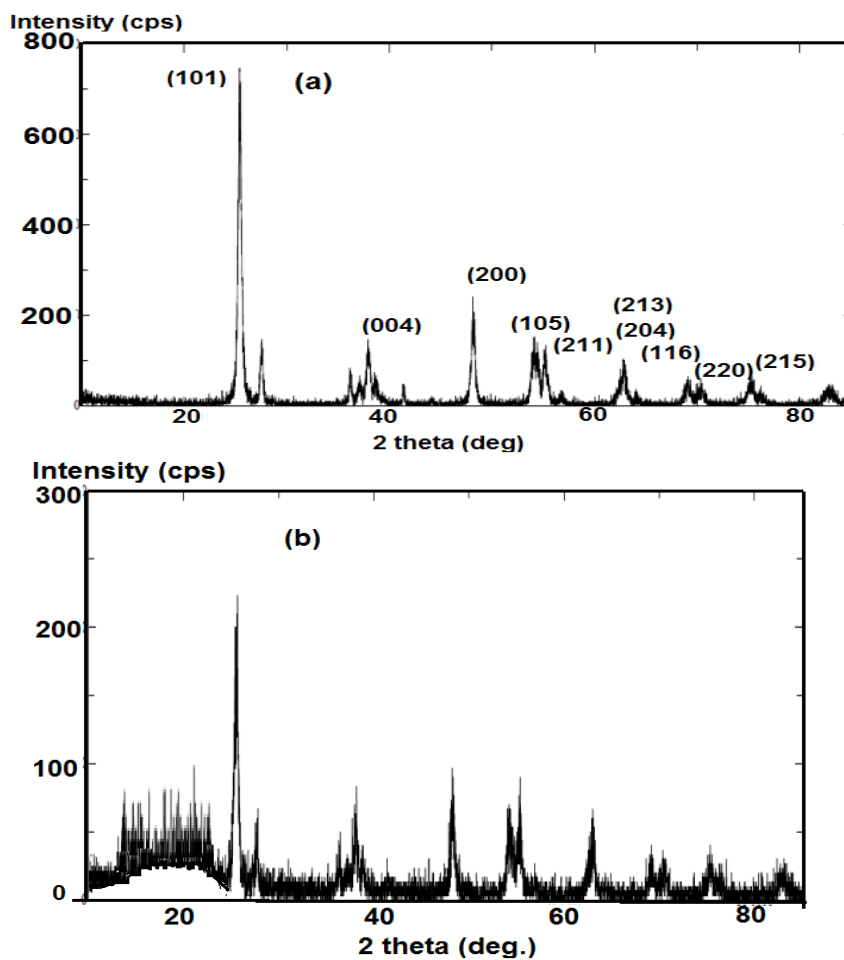


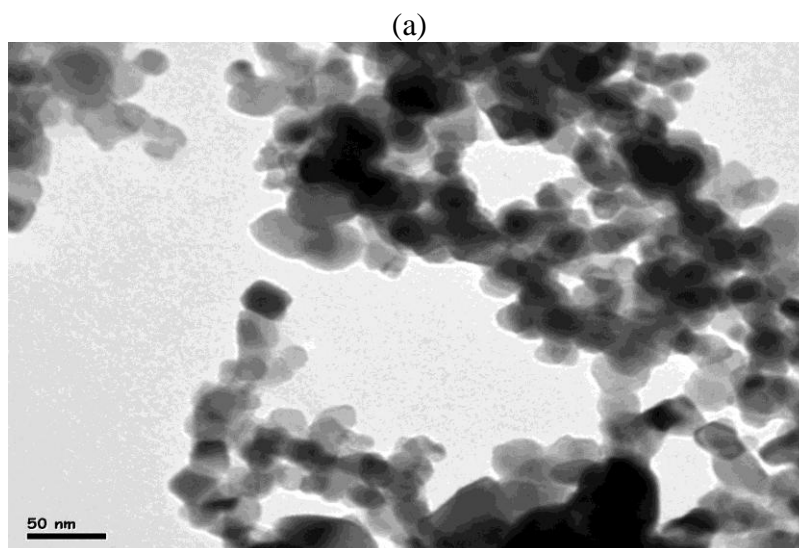
Figure 2. XRD pattern of a) TiO₂ NPs and b) PNa-AMPS /TiO₂ nanogel.

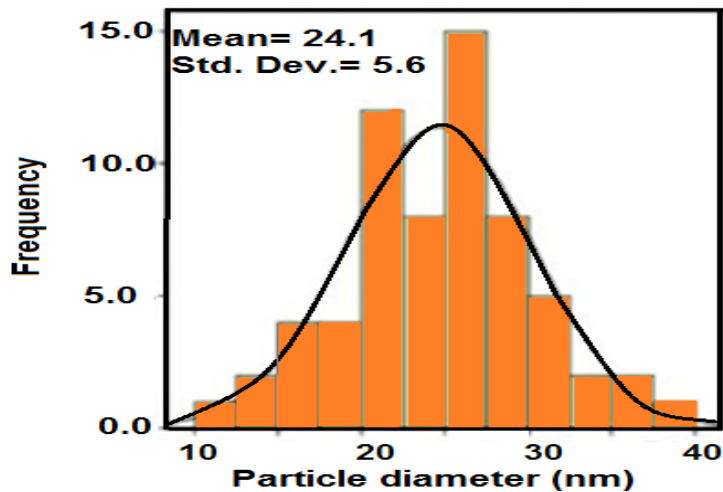
Figure 2a shows the diffractograms for TiO_2 in which Scherrer equation is used to determine the crystalline size from the X-ray line-broadening method. The average crystalline size was found to be approximately 21.76 ± 0.06 nm. Figure 2b displays the XRD patterns of the *PNa-AMPS* / TiO_2 NCs. The appearance of broad amorphous diffraction peak at $2\theta = 15\text{--}35^\circ$ indicates the formation of polymer composite. It was reported that the peak at 2θ of 26.1° with the (101) peak of TiO_2 was attributed to the anatase TiO_2 phase [38]. Careful inspection of diffractograms of the TiO_2 NPs and *PNa-AMPS* / TiO_2 NCs confirms the decreasing of peak intensity of the (101) of TiO_2 that is referred to the surface coverage of the nanoparticles by *PNa-AMPS* nanogel.

3.3. Morphology of *PNa-AMPS*/ TiO_2 nanogel:

The encapsulation of TiO_2 /PVP into *PNa-AMPS* matrix can be evaluated by study the morphological images using transmission electron microscopy (TEM), as represented in Figure 3. Careful inspection of TEM image of the TiO_2 NPs, Figure 3a, showed random in shape (spherical and cubic) nanoparticles which agree in harmony with the previous work [39]. The TEM histogram of the TiO_2 NPs indicated polydispersity of titania nanoparticles as represented in TEM image. Moreover, the TiO_2 NPs histogram determined that the mean particle size of the TiO_2 NPs is approximately 24.1 ± 0.6 nm.

Careful inspection of *PNa-AMPS* / TiO_2 micrograph, Figure 3b, showed core shell morphology in which titania encapsulated the *PNa-AMPS* nanogel. The particle size *PNa-AMPS* / TiO_2 was increased up to 97 nm. This data speculated that the polymerization mechanism plays an important factor for particle size distribution and morphology. The TEM images, Figure 3b, indicated that the TiO_2 NPs encapsulated inside the nanocomposite with different particle size. DLS measurements of *PNa-AMPS* / TiO_2 NCs was represented in Figure 4. The hydrodynamic average particle sizes of *PNa-AMPS* / TiO_2 NCs is 72.2 nm with (Figure 4). The polydispersity value was 1.83, indicating a poly size distribution in aqueous solution.





(b)

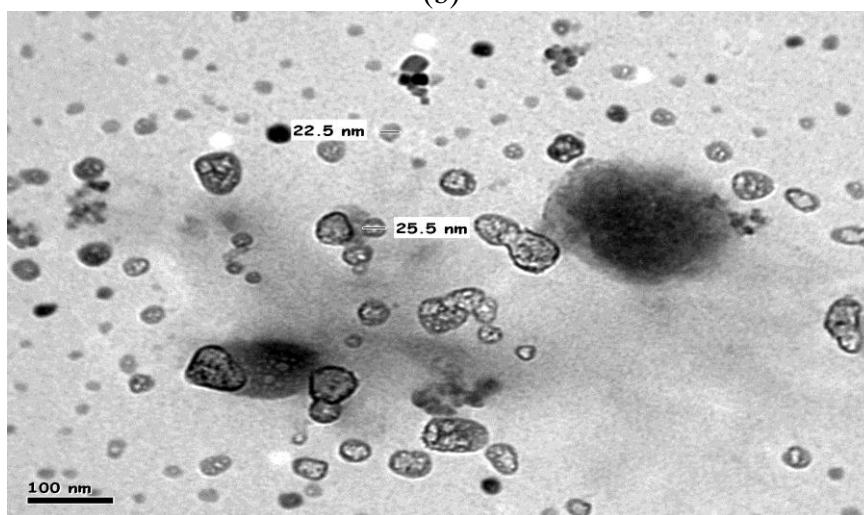


Figure 3. TEM micrographs of a) TiO₂/PVP, and b) PNa-AMPS/TiO₂ nanogel.

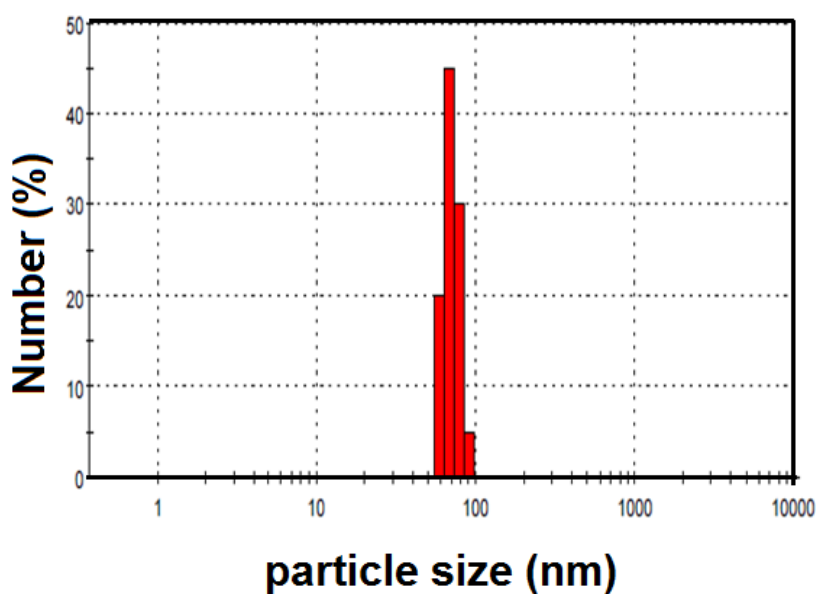


Figure 4. DLS measurements of PNa-AMPS/TiO₂ nanocomposite.

3.4. Polarization measurements

Potentiodynamic curves for steel in 1M HCl solution containing different concentrations of TiO₂ nanoparticles is shown Fig. 5. Both branches of the polarization curve shifted to the lower current densities compared with the uninhibited solution indicating that the TiO₂ nanoparticles labeled as a mixed-type inhibitor. All obtained electrochemical parameters from the polarization curves are quoted in Table 1. It is evident that the addition of nanoparticles to the acidic chloride solution causes a shift in the corrosion potential (E_{cor}) of the steel toward a less noble value and provide a protection of steel towards anodic dissolution and cathodic reduction reaction. The result may be attributed to the adsorption of TiO₂ nanoparticles on the active sites of steel surface with a formation of protective layer, which acts as barrier film for diffusion of the aggressive ions to the steel surface.

This in turn inhibits the anodic dissolution process as well as the cathodic reduction reaction. The inhibition efficiency (IE%) can be calculated by the following relation [33-34]:

$$IE(\%) = 1 - (i_{inhibited} / i_{uninhibited}) \times 100 \quad (1)$$

where $i_{inhibited}$ and $i_{uninhibited}$ are the inhibited and uninhibited corrosion current densities, respectively. The difference in the IE% values clearly indicates that the addition of TiO₂ nanoparticles to 1M HCl solution suppresses the action of the chloride ions and reduces the corrosion rate of steel and increases the protection efficiency.

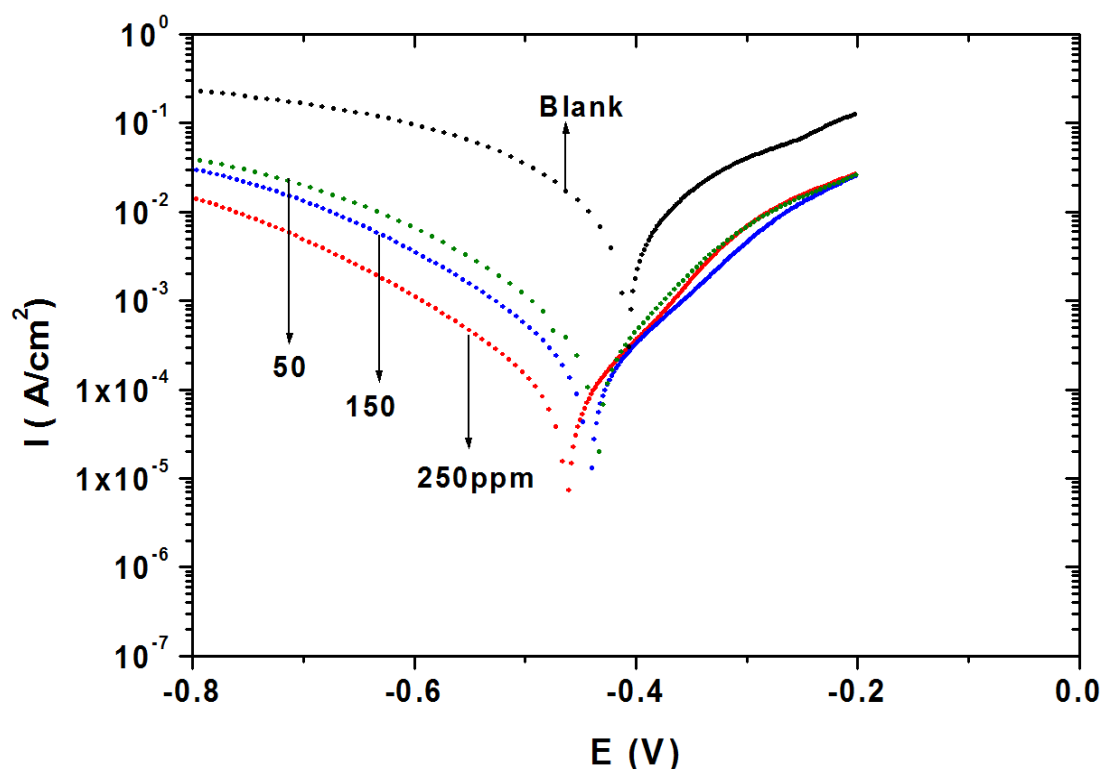


Figure 5. Influence of TiO₂ nanoparticles concentration on the polarization curves for steel in 1.0 M HCl solution.

Table 1. Influence of TiO₂ nanoparticles additions to 1M HCl solution on the protection efficiency values for steel calculated by electrochemical techniques.

	Polarization Method				EIS Method			
	Ba (mV)	Bc (mV)	E _{corr} (V)	i _{corr} (μA/cm ²)	IE%	R _p (Ohm)	Cdl (μF/cm ²)	IE%
Blank	147.00	141.00	-0.4034	745	_____	1.80	334	_____
50ppm	98.53	111.58	-0.4346	283.1	62.0	5.5	198	67.7
150	100.98	111.28	-0.4413	161.1	78.3	8.1	145	77.7
250	79.03	106.84	-0.4620	64.65	91.3	20.2	112	91.0

This indicates high corrosion inhibition effectiveness, which increased with increasing inhibitor concentration. It can be concluded that the higher the inhibitor concentration the higher the inhibition efficiency due to more adsorption of TiO₂ nanoparticles, which provide wider surface coverage on steel surface. The results quoted in Table 1 indicated that the protection performance of the inhibitor increases with increasing concentration. This results can be accounted to the formation of the inhibitive and protective barrier film, which inhibited the chloride ion in the acidic medium from attacking the steel surface.

3.5 EIS measurements

The impedance spectra are characterized by formation of one single capacitive loop in all cases. The diameter of semicircle is strongly dependent upon the concentration of TiO₂ nanoparticles and increases with increasing concentration. These plots give an evidence for increasing the protectiveness of the inhibitive film with increasing the inhibitor concentration. The equivalent circuit shown in Fig. 7 is employed to fit the impedance spectra. R_s represents the solution resistance, a Cdl represents the double layer capacitance and R_{ct} denotes the charge-transfer resistance. The water molecules with high dielectric constant were replaced by TiO₂ nanoparticles with small dielectric constant by adsorption at the steel /solution interface and cause a decrease in the Cdl values [40–42]. The increase in R_{ct} values with increasing of TiO₂ nanoparticles concentration indicated the performance of insulated adsorbed layer formed on steel surface. The formation of an inhibitive and protective film on the steel surface causes a decrease in the anodic dissolution reaction [43] The inhibition efficiency (IE%) can be calculated from the following relation:

$$IE\% = 1 - (R_{ct}^1/R_{ct}^2) \times 100 \quad (2)$$

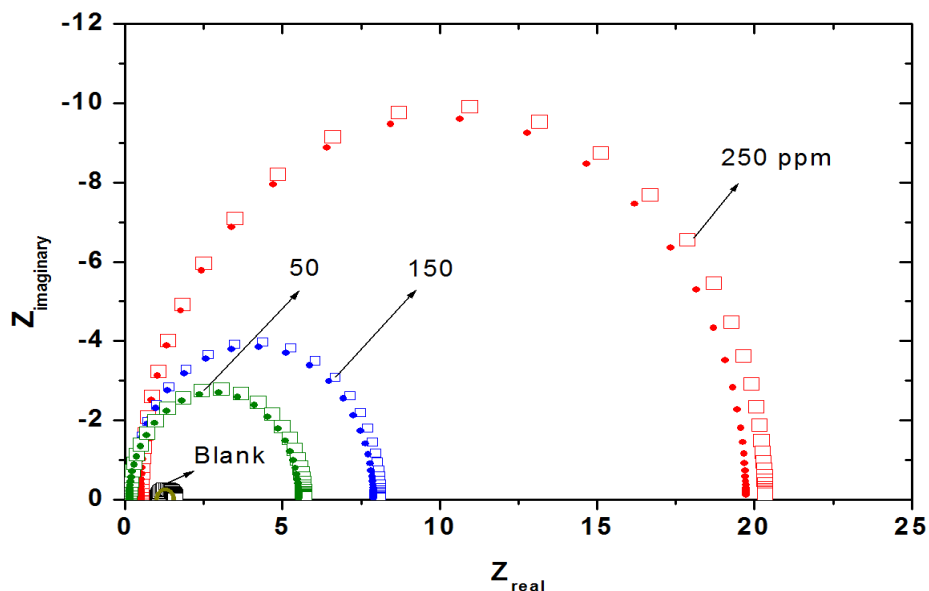


Figure 6. Influence of TiO_2 nanoparticles concentration on the Nyquist plot for steel in 1.0 M HCl solution.

where R_{ct}^1 and R_{ct}^2 are the charge transfer resistances in inhibited and uninhibited solution, respectively. It is evident that IE% increases with increase in the concentration of TiO_2 nanoparticles. The amount of adsorbed TiO_2 nanoparticles on steel surface increased with increasing the inhibitor concentration, which in turn suppresses the corrosion process of steel and consequently increase the inhibition efficiency of the inhibitor. The results obtained here are in consistent with that reported previously for corrosion protection of steel with the addition TiO_2 nanoparticles to epoxy resin in acidic medium [44].

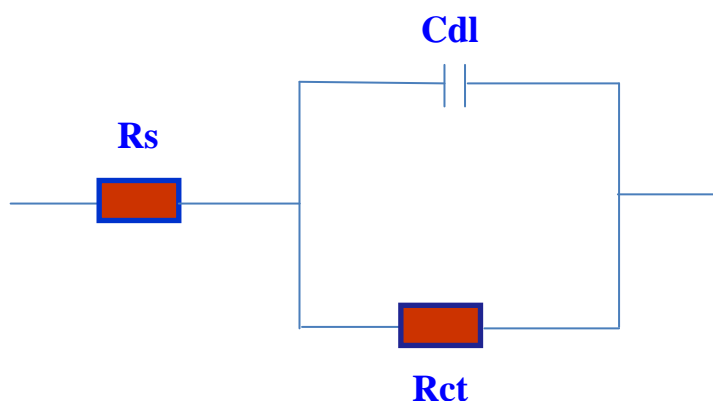


Figure 7. Equivalent circuit used to fit EIS data.

4. CONCLUSIONS

1. Titania, TiO_2 , is encapsulated with PNa-AMPS to prepare nanogel composites.

2. Titania interacts with Na-AMPS to form nanogel composite with nano-size distribution.
3. The TEM and DLS analyses reveal that PNa-AMPS is completely surround the TiO₂-PVP to form core shell structure with will defined morphology.
4. The hydrodynamic average particle sizes of PNa-AMPS /TiO₂ NCs is 72.2 nm with a polydisperse nano size distribution in aqueous solution.
5. All electrochemical measurements showed that TiO₂ nanoparticles had good protective properties for the corrosion of steel in acidic chloride solution.
6. Polarization data reveal that TiO₂ nanoparticles can be classified as a mixed-type inhibitor.
7. The additions of TiO₂ nanoparticles in 1M HCl increase the charge transfer resistance of steel.

ACKNOWLEDGEMENT

The project was financially supported by King Saud University, Vice Deanship of Research Chairs.

References

1. A.D. Paola, E. Garia-Lopez, G. Marci, L. Palmisano, , *J. Hazard. Mater.* 211–212 (2012) 3.
2. Q. Zhang, H. Xu, W. Yan, , *Electrochim. Acta* 61 (2012) 64.
3. D.Y. Wu, M.C. Long, , *Surf. Coat. Technol.* 206 (2012) 3196.
4. C.Y. Wang, J. Li, S.Y. Cai, Z.J. Ning, D.M. Zhao, Q. Zhang, J.H. Su, *Dyes Pigm.* 94 (2012) 40.
5. V.A. Ganesh, A.S. Nair, H.K. Raut, T.M. Walsh, S. Ramakrishna, , *RSC Adv.* 2 (2012) 2067.
6. M.A. Nawi, S.M. Zain, *Appl. Surf. Sci.* 258 (2012) 6148.
7. G.X. Shen, Y.C. Chen, C.J. Lin, *Thin Solid Films* 489 (2005) 130.
8. H. Yun, J. Li, H. Chen, Ch. Lin, *Electrochim. Acta* 52 (2007) 6679.
9. Y. Ohko, S. Saitob, T. Tatsuma, A. Fujishima, *J. Electrochem. Soc.* 148 (2001) B24.
10. M.J. Zhou, Z.O. Zeng, L. Zhong, *Corros. Sci.* 51, (2009) 1386.
11. C.X. Lei, H. Zhou, Z.D. Feng, Y.F. Zhu, R.G. Du, *Appl. Surf. Sci.* 257 (2011) 7330.
12. L. Liu, J.M. Hu, W.H. Leng, J.Q. Zhang, C.N. Cao, *Scr. Mater.* 57 (2007) 549.
13. M.C. Li, S.Z. Luo, P.F. Wu, J.N. Shen, *Electrochim. Acta* 50, (2005) 3401.
14. J. Huang, T. Shinohara, S. Tsujikawa, *Zairyo-to-Kankyo* 46, (1997) 651.
15. S. Raghavan, D. Sameer, S. Sudipta, S. Tadashi, *Sol.St. Lett.* 9 (2006) B1.
16. H. Park, K.Y. Kim, W.Y. Choi, *Chem, Comm.* 3(2001) 281.
17. C.X. Lei, H. Zhou, Z.D. Feng, Y.F. Zhu, R.G. Du, *Appl. Surf. Sci.* 257(2011) 7330.
18. G.X. Shen, Y.C. Chen, L. Lin, C.J. Lin, D., *Electrochim. Acta* 50 (2005) 5083.
19. S. Raghavan, S. Tadashi, *Electrochem. Comm.* 5, (2003) 897.
20. N.F. Fahim, T. Sekino, M.F. Morks, T. Kusunose, *J. Nanosci. Nanotechnol.* 9 (2009) 1803.
21. R. Hahn, J.M. Macak, P. Schmuki, *Electrochem. Commun.* 9 (2007) 947.
22. N.K. Allam, C.A. Grimes, *J. Phys. Chem. C* 111 (2007) 13028.
23. S.V. Lamaka, M.L. Zheludkevich, K.A. Yasakau, R. Serra, S.K. Poznyak, M.G.S. Ferreira, *Prog. Org. Coat.* 58 (2007) 127.
24. D.G. Shchukin, S.V. Lamaka, K.A. Yasakau, M.L. Zheludkevich, M.G.S. Ferreira, H. Mohwald, *J. Phys. Chem. C* 112(2008) 958.
25. D. Borisova, H. Mohwald, D.G. Shchukin, *ACS Nano* 5(2011) 1939.
26. M.G. Mahmoud, R.G. Wang, M. Kato, K. Nakasa, *Scripta Mater.* 53, (2005) 1303.
27. H. Park, K.Y. Kim, W. Choi, *J. Phys. Chem. B.* 106, (2002) 4775.

28. H. Park, K.Y. Kim, W. Choi, *Chem. Commun.* 3, (2001) 281.
29. M.C. Li, S.Z. Luo, P.F. Wu, J.N. Shen, *Electrochim. Acta* 50, (2005) 3401.
30. Y. Ohko, S. Saitoh, T. Tatsuma, A. Fujishima, *J. Electrochem. Soc.* 148 (2001) B24.
31. T. Tatsuma, S. Saitoh, Y. Ohko, A. Fujishima, *Chem. Mater.* 13(2001) 2838.
32. G.X. Shen, Y.C. Chen, C.J. Lin, *Thin Solid Films* 489 (2005) 130.
33. G. A. El-Mahdy, , A. M. Atta, H. A. Al-Lohedan, A. M. Tawfik, and A. A. Abdel-Khalek, *Int. J. Electrochem. Sci.*, 10 (2015) 151.
34. G. A. El-Mahdy, , A. M. Atta, H. A. Al-Lohedan and A.O. Ezzat, *Int. J. Electrochem. Sci.*, 9 (2014) 7925.
35. S. Sathiyarayanan, S. Syed Azim, G. Venkatachari, *Electrochim. Acta* 52 (2007) 2068.
36. Primet, M.; Pichat, P.; Mathieu, M. *J. Phys. Chem.*, 75, (1971) 1216.
37. M.R. Mahmoudian, Y. Alias, W.J. Basirun, M. Ebadi, *Appl. Surf. Sci.* 268 (2013) 302.
38. Y.J. Kwon, K.H. Kima, C.S. Limb, K.B. Shim, *J. Ceram. Proces. Res.* 3(2002) 146.
39. A.R. Rao, V. Dutta, *Sol. Eng. Mater. & Solar Cells* 91 (2007) 1075.
40. A. Popova, E. Sokolova, S. Raicheva, M. Christov, *Corros. Sci.* 45, (2003) 33.
41. S.Y. Sayed, M.S. El-Deab, B.E. El-Deab, B.E. El-Anadouli, B.G. Ateye, *J. Phys. Chem. B.* 107, (2003) 5575.
42. E.E. Oguzie, Y. Li, F.H. Wang, *J. Coll. Interf. Sci.* 310 (2007) 90.
43. F. Bentiss, M. Traisnel, M. Lagrenee, *Corros. Sci.* 42 (2000) 127.
44. T.S. Radoman, J. V. Dzunuzovic, K. B. Jeremic, B. N. Grgur, D. S. Milicevic, I. G. Popovic, E. S. Dzunuzovic, *Mater. Design* 62 (2014) 158.

© 2015 The Authors. Published by ESG (www.electrochemsci.org). This article is an open access article distributed under the terms and conditions of the Creative Commons Attribution license (<http://creativecommons.org/licenses/by/4.0/>).